Origin of magnetic moments in carbon nanofoam

D. Arčon,[1,2,*] Z. Jagličič,[3] A. Zorko,[2] A. V. Rode,[4] A. G. Christy,[5] N. R. Madsen,[4] E. G. Gamaly,[4] and B. Luther-Davies[4]

[1]*Faculty of Mathematics and Physics, University of Ljubljana, Jadranska 19, Slovenia*
[2]*Institute Jozef Stefan, Jamova 39, 1000 Ljubljana, Slovenia*
[3]*Institute of Mathematics, Physics and Mechanics, Jadranska 19, 1000, Ljubljana, Slovenia*
[4]*Laser Physics Centre, Research School of Physicsl Sciences and Engineering, The Australian National University,*
Canberra, ACT 0200, Australia
[5]*Department of Earth and Marine Science, The Australian National University, Canberra, ACT 0200, Australia*

A range of carbon nanofoam samples was prepared by using a high-repetition-rate laser ablation technique under various Ar pressures. Their magnetic properties were systematically investigated by dc magnetization measurements and continuous wave (cw) as well as pulsed EPR techniques. In all samples we found very large zero-field cooled—field-cooled thermal hysteresis in the susceptibility measurements extending up to room temperature. Zero-field cooled (ZFC) susceptibility measurements also display very complex behavior with a susceptibility maximum that strongly varies in temperature from sample to sample. Low-temperature magnetization curves indicate a saturation magnetization $M_S \approx 0.35$ emu/g at 2 K and can be well fitted with a classical Langevin function. M_S is more than an order of magnitude larger than any possible iron impurity, proving that the observed magnetic phenomena are an intrinsic effect of the carbon nanofoam. Magnetization measurements are consistent with a spin-glass type ground state. The cusps in the ZFC susceptibility curves imply spin freezing temperatures that range from 50 K to the extremely high value of >300 K. Further EPR measurements revealed three different centers that coexist in all samples, distinguished on the basis of g-factor and relaxation time. Their possible origin and the role in the magnetic phenomena are discussed.

PACS number(s): 75.75.+a, 75.50.Kj, 75.10.Nr, 75.30.Cr

I. INTRODUCTION

Ferromagnetism is typically regarded as a property of transition metals. These elements have a net magnetic moment because their atoms retain unpaired electrons in unfilled shells even in solids. On the other hand carbon atoms show very strong tendency to pair up their outer-shell electrons in covalent bonds. Therefore, carbon had been dismissed as an element for making magnetic materials for centuries. However, in the last decade several carbon-rich phases have been made that show ferromagnetic behavior. In fullerenes, ferromagnetism was discovered in TDAE-C_{60} (Refs. 1–4) as well as in polymerized C_{60} forms.[5–7] Another class of carbon-based ferromagnets includes various forms of amorphous carbon derived from graphite. Ferromagnetic correlations have, for instance, been observed in activated mesocarbon microbeads, which is mainly composed of miniature graphitic crystallites.[8] Magnetization curves measured at 1.7 K showed a marked hysteresis,[8] which becomes less and less visible with increasing temperature (although still visible at room temperature). The residual magnetization was found to be extremely small (0.016 emu/g) but still larger than any possible ferromagnetic impurity. Independence of magnetic properties and impurity content was later found in highly oriented pyrolytic graphites, with ferromagnetic saturation magnetizations of the order of 10^{-3} emu/g.[9,10] Magnetic correlations were also observed in hydrogenated amorphous carbon (a-C:H),[11,12] which has a significant proportion of sp^3 bonding and C-H groups. Irradiation by protons of energy 2.25 MeV on highly oriented pyrolitic graphite has been shown to trigger room temperature ferromagnetism.[13] In this case ferromagnetism was associated with the mixed sp^3-sp^2 structure stabilized by mono- and dihydrogenated carbon atoms[13,14] or monohydrogenated edges.[15]

Ferromagnetism thus occurs in quite different carbon-derived systems, but it is still unclear which are the most crucial factors in the process of stabilization of magnetic moments and promotion of exchange interactions. The discovery of ferromagnetic response in cluster-assembled carbon nanofoam[16] opens new possibilities to throw some additional light on the carbon-based ferromagnetism. Carbon nanofoam is synthesized by laser-ablation of a graphite or glassy carbon target in an argon atmosphere.[17,18] The "soot" obtained exhibits some remarkable physical properties, including a large surface area of 300–400 m^2/g, comparable to zeolites, and an ultralow density (~ 2–10 mg/cm^3). This is among the lowest gravimetric densities ever reported for a solid; only some recently synthesized silica aerogels are lighter.[19] Electron diffraction of the nanofoams suggests the presence of hyperbolic "schwarzite" layers.[17,20] "Schwarzite" layers are saddle-shaped graphitic layers in which the negative Gaussian curvature arises from the presence of carbon rings larger than six members. The carbon nanofoam shows strong magnetization immediately after the synthesis, most of which is actually lost on a very short time scale immediately after the synthesis. But a fraction of this magnetization is stable even on a very long time scale: a saturation magnetization of $M_s = 0.42$ emu/g at 1.8 K can be measured even 12 months after synthesis.[16]

One of the aims of this work is to elucidate the origin of the magnetic moments in carbon nanofoams in connection with their magnetic behavior. Additionally, we present data demonstrating that the ordering behavior is more complex than initially suspected, and that spin-glasslike type behavior also occurs. There are several different possible factors that could account for the origin of magnetic moments. The presence of carbon rings other than 6-member rings would disrupt the regular alternation of double and single C-C bonds

characteristic of canonical bonding models of the graphite structure, which may cause localization of the π-electron clouds and allow localization of unpaired spins. Additionally, spectroscopic data shows clearly the presence of a substantial fraction of carbons in the sp^3 hybridization state. These carbons are believed to provide cross links between different schwarzite layers. Again, they act as barriers to π-electron delocalization, and could help to trap spins. Still another is the possibility of carbon vacancies in the nanographitic regions. The presence of foreign atoms such as hydrogen or oxygen introduced by the exposure to air could also facilitate spin formation and localization by disrupting the conjugated C-C bond system. Electron paramagnetic resonance (EPR) in combination with magnetization measurements and structural data has proved to be a very powerful technique to study different forms of carbon in the past. We therefore decided to perform a systematic study of different carbon nanofoams by continuous-wave (cw) and pulsed EPR techniques, and to correlate the results with magnetization data. We have identified at least three different centers in all carbon nanofoam samples with a characteristic room temperature g factors: 2.0036, 2.0031, and 2.0016. The concentration of each type of center depends not only on sample characteristics but also on thermal history. There appears to be a transition at about 75 K, which may include charge localization and/or accompanying structural deformation, and reflected in the important EPR spectral redistributions. We discuss the possible origin of different magnetic moments and their role in the magnetic transitions.

II. EXPERIMENTAL DETAILS

Laser ablation has proven to be an efficient method for producing nanoclusters of different atomic content and internal structure.[21] Moreover, the size and the structure have a significant effect upon various nanocluster properties; hence, laser ablation provides a relatively simple experimental avenue to control those properties. To create the nanofoam, we have used an ultrafast laser ablation approach where focused laser pulses following with very high repetition rate (MHz range) ablate a target in an ambient gas environment. The gas serves to confine the ablated atomic plume reducing its expansion velocity while the high pulse rate retaining the atoms at a temperature and density high enough for efficient atom-to-atom sticky collisions that result in cluster formation.

Carbon nanofoam samples were prepared using high power frequency doubled Nd:YVO$_4$ laser operating at the second harmonic (532 nm), with repetition rate 1.5 MHz, pulse duration 12 ps,[22] and focused down to a spot size ~ 15 μm. This gave a maximum incident intensity of 7×10^{11} W/cm^2 with corresponding fluence 8.6 J/cm^2. The ablated mass per pulse was of the order of 10^{-10} g which corresponds to ~ 0.3 mg/s. To avoid crater formation on the target surface and provide steady state ablation conditions, the laser beam was scanned using a constant velocity spiral pattern formed by x-y scanning mirrors. The laser beam was moved at a velocity of 1 m/s (10 laser pulses per spot) over the target surface. To produce the samples of this study, graphite and glassy carbon targets were ablated in a stainless

steel vacuum chamber pumped to a base vacuum of 5×10^{-7} Torr, and then filled with high-purity (99.995%) Ar gas at various pressures in the range 0.2 Torr–200 Torr.

The nanofoam was collected from the inner surface of a 50-mm diameter fused silica SiO$_2$ cylinder located around the plume. An impurity analysis of the carbon nanofoam samples made in different conditions was performed using inductively coupled plasma-atomic emission spectroscopy (ICP-AES). Samples were digested in a small volume of hot concentrated nitric acid and then diluted using ultrapure water (>18 MΩ cm resistivity). Approximately 0.2 g of foam was digested to produce 20 mL of final digest, giving an overall dilution factor of about 100. The digest was then filtered using a 0.45 μm membrane filter to remove particulates and presented to the spectrometer. A Varian Vista Pro axial geometry AES was used. The concentrations of each element measured were calculated from the intensities of specified atomic emission lines relative to those in blank 2% nitric acid and in a multielement standard prepared from commercial single-element standard solutions. Detection limits in solutions as presented ranged from single ppb for 3d transition metals, lanthanides and Mg to tens of ppb for Na, K, Ca, and B-group metals including Al. Corresponding detection limits in the foam were therefore hundreds of ppb to single ppm. ICP-AES impurity analyses are shown in Table I. Similar analysis for ablated glassy carbon and graphite targets suggests that most of the impurities are from the target material but not from the sample handling procedure.

Our previous structural studies of the nanofoam revealed the presence of hyperbolic schwarzite layers[16,17,20] in the clusters forming the foam. Schwarzites are anticlastic (saddle shaped), warped graphitelike sheets, in contrast to the synclastic (ellipsoidally curved) sheets of fullerenes.[23] Microstructural characterization of the foam samples was carried out using high-resolution transmission electron microscopy (HRTEM), electron energy loss spectroscopy (EELS), and radial distribution function (RDF) analysis. The details of structural characterization will be presented elsewhere.

The HRTEM was performed using a JEOL-3000F field emission electron microscope operated at 300 kV with maximum resolution 1.7 Å. Fourier transforms of the images were performed in order to detect any nongraphitic periodicity in the carbon foam. The images had to be taken from appropriate flat and thin areas of material to guarantee the absence of spurious Fourier features arising from dynamical contrast transfer. We obtained images with diffuse diffraction rings corresponding to periodicities that were usually in the range 4–5 Å expected for schwarzite-type curved sheets, but occasionally up to 8 Å (compare 3.5 Å for flat graphite sheets). This distinctively large layer spacing and curved layers have been observed in all the nanofoams studied to date by TEM. However, more systematic study is required in order to ascertain whether there is any systematic correlation between quantitative details of the structure and quantitative magnetic properties.

EELS spectra where collected from both the carbon K edge (280–350 eV) and the low loss (0–50 eV) regions. The fraction of sp^3 bonded carbon atoms was calculated from the carbon K edge[24] assuming that $(sp^2+sp^3)=100\%$. The sp^3 content was found to be in the range 8–20%,

TABLE I. Impurity content in carbon nanofoam material made at various pressures and in a graphite or a glassy carbon target ("SD" =estimated standard deviation). The bottom line presents the percentage of sp^2 bonding assuming $(sp^2+sp^3)=100\%$. Concentrations below the noise level are marked by "—," while Eu, Ho, La Lu, Nd, Sc, Tb, Th, Tm, and U were measured but not included in the table because the concentration was at the noise level for all samples. The results are given in ppm per atom.

Element	10 Torr graphite (1.5 MHz)		50 Torr graphite (1.5 MHz)		200 Torr graphite (1.5 MHz)		50 Torr glassy-C (1.5 MHz)		Glassy-C target		Graphite	
	Conc ppm	SD	Conc ppm	SD	Conc ppm	SD	Conc ppm	SD	Conc ppm	SD	Conc ppm	SD
Al	11	2	13	1	387.2	4.7	28	1	2.12	0.13	13.45	0.13
Ca	313	3	532	2	386.7	0.7	709	7	24.71	0.28	117.9	0.95
Ce	—	0.03	—	0.53	—	0.31	—	0.42	0.45	0.03	1.65	0.03
Co	—	—	2.2	0.5	2.2	0.2	1.3	0.2	0.04	0.01	4.05	0.06
Cr	5.91	0.09	3.05	0.07	1.76	0.09	4.7	0.1	0.13	0.01	0.86	0.01
Cu	13.7	0.3	5.9	0.2	20.5	0.2	7.0	0.2	1.27	0.01	8.87	0.02
Dy	—	0.15	—	0.02	—	0.08			—	—	0.04	0.01
Er	—	—	—	—	0.05	0.01	—	—	—	0.01	0.04	0.00
Fe	64	0.5	174	1	133.8	0.3	159	2	4.47	0.08	167.7	0.41
Gd	—	—	—	—	0.17	0.02	—	—	—	0.00	0.09	0.00
K	54.4	0.2	10.4	0.9	10.6	0.2	20.2	0.3	1.30	0.03	8.25	0.07
Mg	5.67	0.05	20.0	0.2	10.94	0.04	26.9	0.2	1.74	0.02	11.07	0.03
Mn	0.62	0.07	0.39	0.02	0.42	0.01	0.36	0.01	0.02	0.00	1.20	0.01
Na	63.6	0.5	137	2	41.3	0.3	71	1	1.86	0.04	19.91	0.11
Ni	29.8	1.6	37.0	0.1	28.8	0.3	25.4	0.9	0.76	0.03	47.54	0.24
Pb	—	13.21	—	4.24	—	4.44			—	0.23	—	0.08
Pr	—	1.78	—	0.63	—	0.33	—	0.98	—	0.02	0.09	0.00
Ti	0.33	0.07	8.09	0.03	7.38	0.04	5.23	0.04	1.08	0.01	12.80	0.17
V	0.4	0.1	4.3	0.1	3.5	0.1	4.12	0.06	0.01	0.00	9.14	0.13
Y	—	—	—	—	0.08	0.00	—	—	—	0.00	0.23	0.00
Yb	—	0.05	—	0.00	—	0.01	—	0.03	—	0.00	0.01	0.00
Zn	23.4	0.5	92	1	31.4	0.3	92.0	0.6	2.13	0.05	2.10	0.08
sp^2 (%)	81.9%		87.0%		92.3%		85.7%		100%		100%	

the results for particular samples are presented in Table I. There was no clear dependence of the proportion of sp^3 bonding or the cluster size on the Ar pressure in the experiments. The low loss region contains plasmon loss peaks, which were used to approximate the volume density.[25] The individual cluster density was found to be in the range 1.55–1.90 g/cm³, close to our earlier estimate of 1.9 g/cm³.[17]

EPR measurements were performed on a commercial Bruker E580 spectrometer. Continuous wave (cw) measurements were done on a Varian dual resonator and Oxford continuous flow ESR 900 cryostat. In order to avoid the influence of adsorbed gases we first evacuated samples at moderated temperature (around 60 °C) and then sealed them under dynamic vacuum to EPR quartz tubes for further experiments. Pulsed EPR experiments were on the other hand performed using a Bruker dielectric resonator, ER 4118X-MD5. A typical $\pi/2$ pulse length used in our experiments was 16 ns. For the relaxation studies inversion-recovery technique was applied with signal detection either via free-induction decay (FID) or echo signal. In all experiments we used appropriate phase cycling sequences to remove unwanted signals. Direct current (dc) magnetization measurements were performed on a quantum design SQUID magnetometer in a magnetic field of 100 Oe down to a temperature of 2 K. In order to avoid carbon nanofoam powder movement inside the holder during the temperature and field scans, we pressed the sample between the two caps of the capsule. During the field scans the temperature stability was better ±0.02 K.

III. RESULTS AND DISCUSSION

A. Magnetic measurements

We begin our discussion with the dc magnetic susceptibility measurements, which are summarized in Figs. 1–3. In all experiments we applied exactly the same cooling protocol: first measurement was taken after zero-field cooling to 2 K and in the second run the measurements were taken under field-cooled conditions. Room temperature susceptibilities slightly vary from sample to sample but they are all
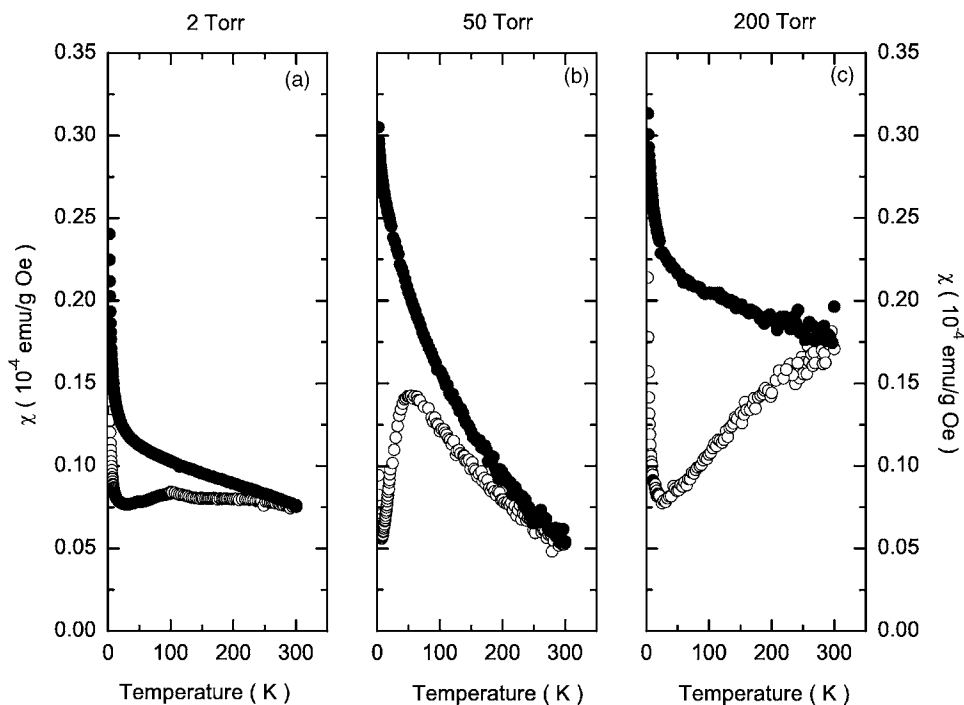
FIG. 1. A temperature dependence of zero-field cooled and field-cooled dc magnetic susceptibilities for different carbon nanofoam samples: (a) sample prepared at 2 Torr Ar pressure (sample mass was 10.4 mg), (b) 50 Torr Ar pressure (sample mass was 10.7 mg), and (c) 200 Torr Ar pressure (sample mass was 8.6 mg). In all cases solid circles stand for FC measurements, while open circles represent ZFC measurements. The magnetic field was in all cases set to 100 Oe.

of the order of 10^{-5} emu/gOe. We note that we also measured a sample prepared in 10 Torr Ar atmosphere, which showed similar behavior to the one prepared in 2 Torr Ar. In what follows we will distinguish three types of temperature behavior, each of which was encountered in several carbon-nanofoam samples.

All samples show very large field-cooling dependence below room temperature: $\chi(T)$ is larger under field-cooling (FC) conditions when compared to values measured under zero-field cooling (ZFC) conditions (Fig. 1). Note that the true coincidence between FC and ZFC measurements is expected to be observed in carbon nanofoam samples only well

above room temperature, i.e., at temperatures currently inaccessible by our experimental equipment. While field-cooled dependences typically show monotonic increase of the magnetic susceptibility with decreasing temperature, the zero-field data displays much more complex behavior. The zero-field cooled data exhibit a maximum and a low-temperature Curie upturn with progressive cooling. These stationary points are observed for all Ar pressures of synthesis, if the maximum for 200 Torr Ar is taken to be near 300 K (Fig. 1). Although the qualitative behavior is the same for all synthesis pressures, the quantitative data vary nonmonotonically with Ar pressure. The temperatures of minimum and maxi-
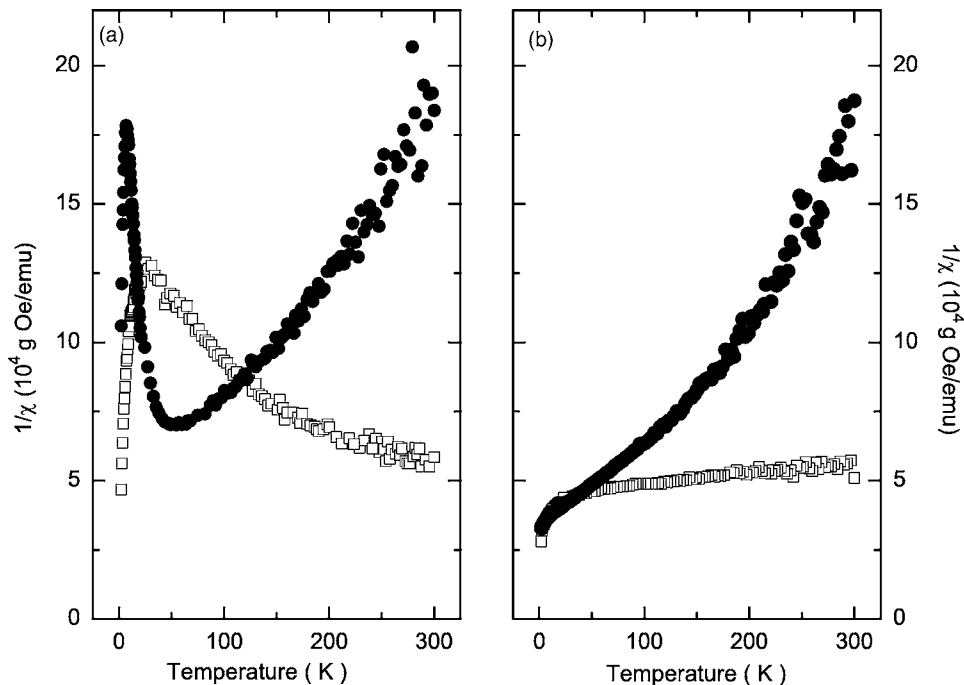

FIG. 2. Temperature dependence of the inverse magnetic susceptibilities (a) zero-field-cooled data (b) field cooled data. Open squares stand for the data measured on 200 Torr sample (mass 8.6 mg), while solid circles stand for the measurements on 50 Torr sample (mass 10.7 mg). Magnetic field was in all cases set to 100 Oe.
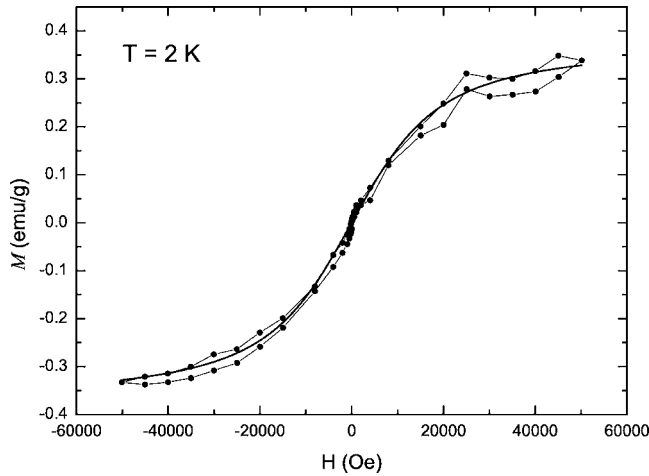
FIG. 3. Magnetic moment versus magnetic field for a selected (prepared in 200 Torr Ar atmosphere; samples mass was 8.6 mg) sample at 2 K (circles). A solid line represents a fit to a Langevin function [Eq. (1)].

mum susceptibility and room-temperature susceptibility all appear to be lower for $P=50$ Torr than for lower or higher pressures. At very low temperatures we find in both the zero-field cooled as well as field-cooled susceptibility a slight Curie-type enhancement of the susceptibility proving the presence of small amount of unpaired "defect" states. Even for the field-cooled samples, plots of reciprocal susceptibility (Fig. 2) in the entire temperature range clearly deviate from a simple Curie-Weiss law (apart from the low-temperature contribution mentioned before).

The behavioral complexity becomes very pronounced in zero-field cooled experiments. In these experiments we find apparent Curie-Weiss behavior only at temperatures sufficiently far above the susceptibility maximum. This is near 100 K for the 2 Torr sample [Fig. 1(a)], very marked at around 50 K for the 50 Torr sample [Fig. 1(b)] and not obvious but perhaps shifted to temperatures above 300 K for the 200 Torr sample [Fig. 1(c)]. Note the near-linear trend of the inverse susceptibility for the 50 Torr sample in Fig. 2(b) at $T>50$ K, and compare it with the behavior at lower temperatures. The existence of maxima in the zero-field cooled experiments can be also a consequence of competing inter-actions and/or low dimensionality of the magnetic system. We note here a striking similarity between the ZFC suscep-tibility measured in our system and that of the crystalline organic radical systems "BIP-BNO" and "BIP-TEMO,"[26,27] which is characterized by a low-dimensional antiferromag-netic interactions. Another system that exhibits some simi-larities in its magnetic properties to the nanofoam is the modified graphite of (Ref. 28). This material shows a satu-rated magnetic moment up to 0.58 emu/g (2 K), an initial susceptibility of about 6×10^{-5} emu/gOe, divergent ZFC and FC magnetization curves with multiple magnetic transi-tions, and what appear to be ferromagnetic domains imaged in magnetic force microscopy.

The temperature dependences of the measured suscepti-bilities (Figs. 1 and 2) thus point to an unconventional type of magnetism in carbon nanofoams, which cannot be easily

explained within some standard model. For instance, we note that zero-field–field-cooled hysteresis can be observed in su-perparamagnetic particles below the blocking temperature.[29] This would in our case imply extremely high blocking tem-perature, far exceeding room temperature. However, the presence of maxima (Fig. 1) in the zero-field cooled data seems to speak against this possibility. On the other hand such behavior is characteristic also of spin glasses.[30] The complexity of the behavior signals the importance of com-peting magnetic interactions between magnetic moments. The susceptibility maximum could thus correspond to the freezing temperature T_f of the spin glass, which is near 50 K for the 50 Torr sample, but appears to be at the very high temperature of at least >300 K for the 200 Torr sample [Fig. 2(b)].

All samples show anomalous hysteresis in the field curves (Fig. 3) at low temperature. Saturation magnetization corre-sponds to $M_S\approx0.385$ emu/g at 2 K and is comparable to what has been measured in other disordered carbon materials.[31,32] We again stress that this value is an order of magnitude larger than the expected saturated magnetization of any possible iron impurity (according to impurity analysis presented in Table I we estimate the upper limit to be around 0.014 emu/g). This proves that the magnetic phenomena we are studying in this work are indeed an intrinsic property of the carbon nanofoam and not some extrinsic effect. The mag-netization curves (Fig. 3) can be satisfactory fitted with a Langevin function $L(y)$ valid for classical (i.e., $S\rightarrow\infty$) spins

$$M = M_S L(y) = M_S\left(\coth y - \frac{1}{y}\right), \qquad (1)$$

where is parameter $y=\mu B/k_B T$. A fit to the experimental data leads to a magnetic moment $\mu=12.5(2)\mu_B$ suggesting a clus-tering of the $S=1/2$ spins.

We also note that, a very steep increase in the magnetic moment when cycling with a field around 0 Oe (i.e., high initial susceptibility) has been noticed. The contribution of this part is about ~0.05 emu/g and is still larger than the one expected for the iron impurity phase.

Thus, unless there is some unusual Fe-impurity aggrega-tion in carbon nanofoam samples the measured sample mag-netization is of intrinsic origin. The large thermal hysteresis in the ZFC-FC measurements (Fig. 1) is likely to be associ-ated with the existence of spin clusters. The interactions be-tween these clusters lead to spin freezing processes in cor-roboration with our idea of spin-glasslike state. We note that this kind of behavior gradually disappears with increasing temperature and is barely discernible (if at all) at room tem-perature.

Based on our magnetization measurements we can make the following conclusions about carbon nanofoam samples studied in this work:

(i) The samples are magnetically highly inhomogeneous. There are at least two contributions to the total magnetic moment: a contribution with a steep increase around 0 Oe and $M_S\approx0.05$ emu/g, and a major phase with $M_S\approx0.35$ emu/g. The iron impurity is, on the basis of the im-purity analysis (Table I), expected to participate in the total

magnetization to the extend of only 0.014 emu/g, 25 times lower than observed.

(ii) The magnetic moments seem to form clusters leading to an average magnetic moment 12.5 μ_B.

(iii) Magnetic properties are strongly dependent on the thermal history, i.e., whether the samples were cooled under zero-field or field conditions.

(iv) Such thermal history effects are consistent with a spin glass picture where the system can exist in many different roughly equivalent spin configurations rather than one unique long-range ordered scheme. The spin freezing temperature is unusually high (50–300 K) compared with that of typical spin glasses such as $Eu_{0.2}Sr_{0.8}S$ (0.7 K) and Cu:Mn (10–15 K).[30] The frustration that leads to spin glass formation in carbon nanofoam samples may be either geometrical or can be due to the local variations of the exchange couplings between magnetic moments. Both effects are likely to be a direct consequence of the carbon nanofoam structures based on different carbon rings or the competition between sp^2 and sp^3 carbons.

(v) A rapid increase in susceptibility at very low temperatures implies that some spins remain unfrozen at T_f and do not couple strongly at all, thus showing a near zero T_c. The complexity of $\chi(T)$ behavior therefore suggests that the nanofoam contains at least two distinct types of spin-bearing region, one with frustrated coupling and one with negligible coupling. Likely the origin of these moments are carbon dangling bonds that are exchange couple with other moments.

B. Electron paramagnetic resonance

Though the magnetization measurements enable us to study the macroscopic nature of the magnetic ordering of the carbon nanofoams, they do not provide us with diagnostic information as to the origin of the magnetic moments. We therefore decided to investigate the samples using EPR. A typical room temperature cw EPR spectrum measured in carbon nanofoam sample synthesized under 2 Torr Ar atmosphere is shown in Fig. 4. Samples prepared under different Ar atmospheres had similar lineshapes. The effective g-factors range between 2.0029(3) for the sample prepared at 50 Torr Ar atmosphere and 2.0032(3) for samples prepared at 2 Torr Ar atmosphere. Linewidth ranged between 1.5 G (sample prepared at 200 Torr) and 2.1 G (sample prepared at 10 Torr). We stress that in air-exposed samples the measured EPR linewidth is considerably broader. For instance, in sample prepared under 50 Torr Ar atmosphere and exposed to air, the measured linewidth is about 8 G. After evacuation of the sample the linewidth shrinks to 1.9 G. This suggests that the carbon nanofoam surface adsorbs gases like oxygen, and coupling to paramagnetic oxygen is then responsible for the line broadening. In order to avoid influence of physisorbed gases on the magnetism in carbon nanofoam we decided to work on samples that were sealed into quartz tubes under high vacuum prior to the EPR experiments.

The EPR lineshape strongly deviates from a simple Lorentzian lineshapes. An integrated EPR spectrum is shown in the inset to Fig. 4 in order to demonstrate the extension of the signal far beyond the range expected for Lorentzian line-
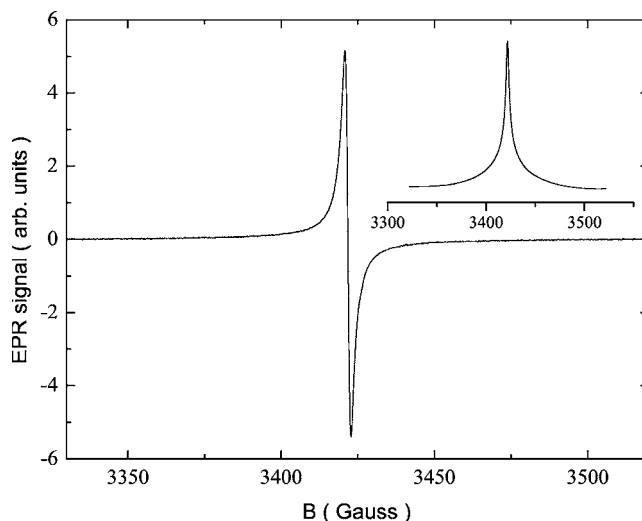

FIG. 4. A room temperature EPR spectrum measured in carbon nanofoam synthesized under 2 Torr Ar pressure. In the inset we show the integrated EPR spectrum. Note large wings in the signal atypical even for Lorentzian lines.

shape. This suggested either very complex spin correlation function in the exchange coupled system or a superposition of several different overlapping components. Later on we discuss pulsed EPR experiments, which were conducted in order to elucidate this matter.

We found in some samples an additional EPR signal shifted to lower fields (Fig. 5). This signal is at room temperature shifted for about 400 G while the width of this signal is about 330 G. The shift is strongly temperature dependent and decreases with increasing temperature (inset to Fig. 5). Such signals are characteristic of ferromagnetic resonance, where the shift is caused by demagnetizing effects and/or magnetic anisotropy and its temperature dependence is the result of the temperature dependence of the magnetization. We have to admit however that the appearance of this
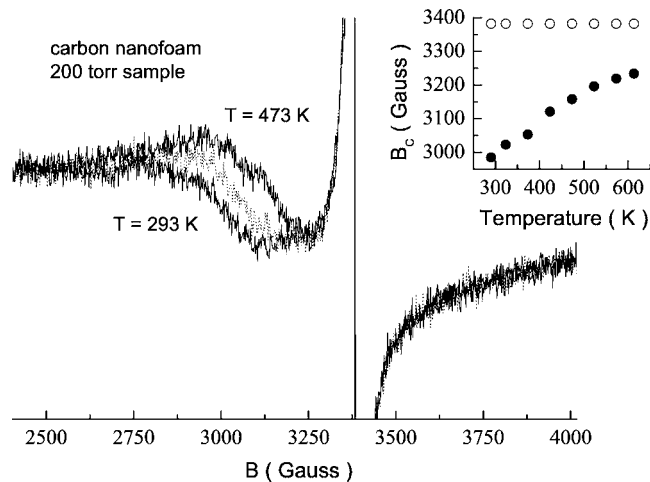

FIG. 5. Temperature evolution of the additional EPR signal shifted to lower fields measured at 293 K, 373 K (dotted line), and at 473 K. A temperature dependence of the center of the shifted line (solid circles) is shown in the inset and compared with the position of the $g=2.0032$ line (open circles).
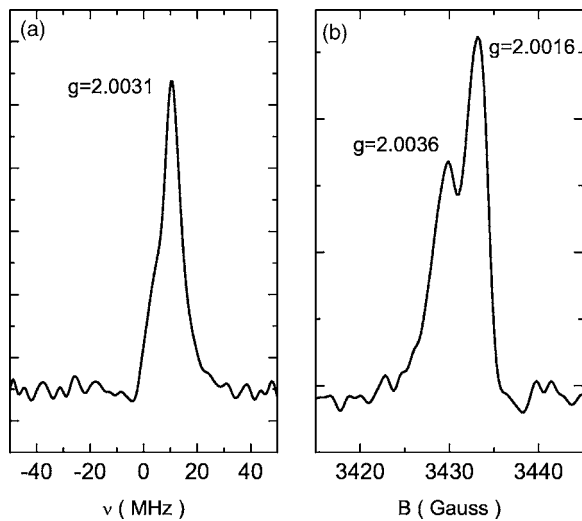
FIG. 6. (a) A Fourier transform of a free induction decay signal measured in carbon nanofoam synthesized under 2 Torr Ar atmosphere. Here $T=295$ K. (b) A spectrum obtained by a field sweep echo detection technique at $T=80$ K. The sample was in both cases carbon nanofoam synthesized under 2 Torr Ar atmosphere.

signal is sporadic; we could not find it in every sample. The reason for this may lie in the large dependence of remanent magnetization on the thermal and magnetic history, i.e., a direct reflection of the spin-glasslike state. Another possible origin of this line could be the presence of some magnetic iron impurity phase. However, from the results presented in Table I one can calculate that the intensity of the low-field line by almost two orders of magnitude exceeds the intensity expected for such impurities.

Given the complexity of the cw EPR lineshape (Fig. 4) we decided to perform additional pulsed EPR experiments. To our surprise, we found that the total EPR signal is in fact a superposition of at least three signals. The first signal can be easily detected with free induction decay. A Fourier transform of this signal is shown in Fig. 6(a). The effective g factor of this signal is 2.0031, i.e., the same as in cw experiments. Linewidth at half height $\delta\nu_{1/2}=\frac{2}{T_2}=9.3(2)$ MHz, which is also in a good agreement with the measured peak-to-peak cw linewidth, i.e., $\Delta B_{pp}=\frac{\delta\nu_{1/2}}{\gamma\sqrt{3}}=1.9$ G. Therefore the central contribution to the cw EPR signal can be also detected by free induction decay. On the other hand, we can also find echo signals. A field-sweep echo detected spectrum is shown in Fig. 6(b). Here two different resonance signals can be identified with effective g-factors 2.0036 and 2.0016. We emphasize at this point that the same three g-factor values appear in all carbon nanofoam samples studied in this work. This suggests that the local structural motifs around the paramagnetic defects are very similar irrespective of the details of the synthesis procedure.

We believe that these two extra signals may be responsible for the deviation of the cw EPR lineshape from a simple Lorentzian line (Fig. 4). We comment however that the tails of the cw EPR spectrum may not be accessible to the pulsed EPR experiments due to their very short relaxation times.

On comparing spectra for different samples, we found that the relative proportion of the $g=2.0016$ and $g=2.0036$ lines
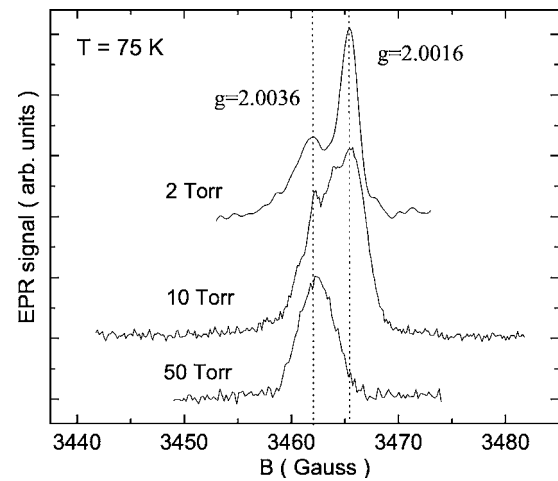

FIG. 7. A variation of the field-sweep EPR spectra measured at 75 K in samples prepared under different Ar atmosphere. Note the disappearance of the $g=2.0016$ line and gradual growing of the $g=2.0036$ line.

at 75 K changed systematically on going from samples prepared at 2 Torr to 50 Torr Ar atmosphere (Fig. 7). A narrow $g=2.0016$ line gradually lost intensity with increasing Ar pressure, and in samples prepared at high pressure, only a $g=2.0036$ line can be seen. The intensity of the $g=2.0036$ signal rapidly disappears above 80 K and at high temperatures only the $g=2.0016$ has been measured (Fig. 8).

The analysis above suggests a complex ground state of carbon nanofoams with at least three different types of center. The most abundant center has a g factor 2.0031, is responsible for the central part of the cw EPR spectrum and can be also seen in free induction decay experiments. The other two centers are likely responsible for the background of the cw EPR line and can be only distinguished in echo experiments. We emphasize that all three g-factor values are characteristic of carbon-based defects. Nevertheless, we also
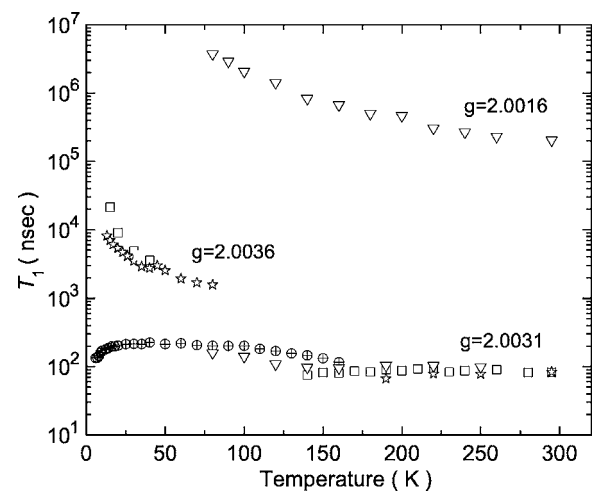

FIG. 8. A temperature dependence of the electron spin-lattice relaxation times measured in different carbon nanofoam samples and different signals (see text for details). Here ($\triangledown$) stands for experiments on 2 Torr sample, ($\star$) for 10 Torr, ($\oplus$) for 50 Torr, and finally ($\square$) for 200 Torr experiments.

checked samples for possible magnetic impurities. The most likely candidates would be different iron complexes, in particular iron oxide or iron carbide particles. The magnetic resonance signals for these two systems are typically very broad (measured EPR linewidths are 1540 G and 3930 G in Fe_3O_4 and Fe_3C nanoparticles respectively)[33–35] and shifted to lower resonance fields as expected for ferromagnetic resonance. We stress that the total analyzed Fe (see Table I) is so low that even if all the iron was in such compounds, we would have difficulties in observing the signals due to sensitivity problems. Our EPR experiments do not detect any noncarbon magnetic impurity in carbon nanofoam samples.

For a complex, noncrystalline material with several different local atomic environments such as the nanofoam, it is necessarily difficult to provide rigorous structural characterization. At best, a picture of the local environments may be evolved by collating various spectroscopic data. In an attempt to shed some additional light on the contributions of the three centers to the observed magnetism, we decided to measure also spin-lattice relaxation times T_1 on different samples. Results are summarized in Fig. 8. We first note that all centers have very different relaxation times, which differ by orders of magnitude, but they do not vary substantially from sample to sample. This supports the conclusion that they correspond to unpaired spins in quite different structural environments. The narrow component with a g-factor value 2.0031 has the shortest T_1 of the order of several 100 ns, the low temperature signal at 2.0036 has T_1 in the range of several 10 μs while $g=2.0016$ signal has T_1 of the order 200 μs already at room temperature (at low temperatures it becomes several ms and thus even difficult to measure). Such different T_1 values prove that these centers are not capable of establishing a common spin temperature, or in other words they do not interact significantly with each other. Therefore, they can be regarded as three independent spin systems.

The very long spin-lattice relaxation time of the $g=2.0016$ line suggests that the local field dynamics in this part of the sample is strongly suppressed. Defects associated with this line should be very diluted and definitely cannot contribute to any sort of magnetic phenomena. We speculate on the basis of the observed changes of $g=2.0016$ and $g=2.0036$ signal intensities (Fig. 7) that these two centers have a very similar spatial location. However, note that the increases in the synthesis Ar pressure is observed to cause replacement of the $g=2.0016$ resonance by the $g=2.0036$, with a relaxation time nearly four orders of magnitude shorter. The echo of the $g=2.0036$ signal also rapidly disappears above 80 K, i.e., above the temperature of the susceptibility maximum. Shortening of the relaxation times cannot solely account for the rapid disappearance of this particular component and one thus has to consider a signal (and consequently charge) redistribution at this temperature. Such redistribution could for instance be due to charge localization below 80 K. On the other hand the near temperature independence of the spin-lattice relaxation time can be taken as an evidence for the strong delocalization of the $g=2.0031$ spins. One may thus propose that that $g=2.0016$ and $g=2.0036$ resonances originate from trapped unpaired electrons.

The transformation from a "low-g" to a "high-g" state is likely due to change in the bonding geometry of the carbon

carrying the unpaired spin. High g factors in the range between 2.0030 and 2.0045 have been found for spectra measured in polymerlike[36,37] or diamondlike films.[38] We deduce that our higher g-factor signals arise from sample regions with some sp^3 character. On the other hand the lower g factor 2.0016 is rather uncharacteristic for amorphous carbon compounds. We note however that g-factors lower than the free-electron value ($g_e=2.002\,32$) are characteristic of fullerenes, with more profound sp^2 character. It is thus possible that this part of the signal comes from sample regions with a curved layer structure, while the two high-g signals arise from the more sp^3-like regions. Further theoretical investigations on the effect of the curvature on the g-factors of the carbon-based defects are needed to support this point.

We note that a transformation of the EPR spectral intensity in which the spins shift from low-g, "sp^2-like" centers in the carbon sheet to environments that are more "sp^3-like" (characterized by higher g values) may be a result of a reduction in C-C-C bonding angle around a 3-coordinate carbon away from 120° and towards $\cos^{-1}(\frac{-1}{3}) \approx 109.47°$. The rearrangement of the bonding electrons that is involved may either cause relocation of the unpaired spin to a more buckled part of the sheet, or may cause buckling of the sheet without relocation of the spin. In either case, the shorter relaxation time in the non-planar environment then allows a frustrated mixture of ferro- and antiferromagnetic couplings between spins that reduces the low-temperature susceptibility. The $g=2.0031$ resonance with very short relaxation time may also couple to the $g=2.0036$ spins and facilitate glass formation.

IV. CONCLUSIONS

In conclusion we have systematically studied magnetic properties of carbon-nanofoam samples prepared under different conditions (Ar pressures). Magnetic susceptibility data shows large differences between ZFC and FC experiments that are consistent with formation of a spin glasslike state with unusually high freezing temperature. There is an additional paramagnetic component in the material that gives a Curie lawlike increase in χ at very low T. Magnetic inhomogeneity is supported by detailed EPR studies, where we recognized three different types of center. One type has a g factor 2.0016 and a very long relaxation time of the order of 1 ms, which renders it unlikely to participate in magnetic ordering. However reduction in temperature of the sample, or increase of the gas pressure of synthesis, cause this center to be replaced by a different type with $g=2.0036$, T_1 of the order of 0.1–1 μs. The crossover occurs at temperatures similar to that where the magnetic susceptibility maximum is observed, and coupling of these centers may be vital for spin freezing. The third type have $g=2.0031$ and ca. 100 ns relaxation time, is present at all temperatures, and may due to its delocalized nature facilitate coupling. The higher g factors (>2.003) are typical of amorphous carbon systems with significant sp^3 character, i.e., strongly nonplanar parts of a carbon sheet. There are indications of a ferromagneticlike EPR signal, but this is not present in all samples.

Note added. Seven out of nine authors of Ref. 6 retracted

from the results on ferromagnetic behavior of polymerized fullerenes with the Curie temperature around 500 K published in Ref. 6. See Ref. 39.

*Corresponding author. Present address: Institute Jozef Stefan, Jamova 39, 1000 Ljubljana, Slovenia. Electronic address: denis.arcon@ijs.si

[1] P.-M. Allemand, K. C. Khemani, A. Koch, F. Wudl, K. Holczer, S. Donovan, G. Gruner, and J. D. Thompson, Science **253**, 301 (1991).

[2] D. Arčon and R. Blinc, *Structure and Bonding* (Springer-Verlag, Berlin/Heidelberg, 2004).

[3] R. Blinc, P. Jeglič, T. Apih, J. Seliger, D. Arčon, J. Dolinšek, and A. Omerzu, Phys. Rev. Lett. **88**, 086402 (2002).

[4] D. Arčon, P. Cevc, A. Omerzu, and R. Blinc, Phys. Rev. Lett. **80**, 1529 (1998).

[5] Y. Murakami and H. Suematsu, Pure Appl. Chem. **68**, 1463 (1996).

[6] T. L. Makarova, B. Sundqvist, R. Höhne, P. Esquinazi, Y. Kopelevich, P. Scharff, V. Davydov, L. S. Kashevarova, and A. V. Rakhmanina, Nature (London) **413**, 716 (2001).

[7] V. N. Narozhnyi, K.-H. Müller, D. Eckert, A. Teresiak, L. Dunsch, V. A. Davydov, L. S. Kashevarova, and A. V. Rakhmanina, Physica B **329**, 1217 (2003).

[8] C. Ishii, Y. Matsumura, and K. Kaneko, J. Phys. Chem. **99**, 5743 (1995).

[9] Y. Kopelevich, P. Esquinazi, J. H. S. Torres, and S. Moehlecke, J. Low Temp. Phys. **119**, 691 (2000).

[10] P. Esquinazi, A. Setzer, R. Höhne, C. Semmelhack, Y. Kopelevich, D. Spemann, T. Butz, B. Kohlstrunk, and M. Lösche, Phys. Rev. B **66**, 024429 (2002).

[11] R. Blinc, D. Arčon, P. Cevc, I. Pocsik, M. Koos, Z. Trontelj, and Z. Jagličič, J. Phys.: Condens. Matter **10**, 6813 (1998).

[12] D. Arčon, J. Seliger, R. Blinc, I. Pocsik, and M. Koos, Solid State Commun. **107**, 349 (1998).

[13] P. Esquinazi, D. Spemann, R. Höhne, A. Setzer, K.-H. Han, and T. Butz, Phys. Rev. Lett. **91**, 227201 (2003).

[14] K. Kusakabe and M. Maruyama, Phys. Rev. B **67**, 092406 (2003).

[15] M. Fujita, K. Wakabayashi, K. Nakada, and K. Kisakabe, J. Phys. Soc. Jpn. **65**, 1920 (1996).

[16] A. V. Rode, E. G. Gamaly, A. G. Christy, J. G. Fitz Gerald, S. T. Hyde, R. G. Elliman, B. Luther-Davies, A. I. Veinger, J. Androulakis, and J. Giapintzakis, Phys. Rev. B **70**, 054407 (2004).

[17] A. V. Rode, S. T. Hyde, E. G. Gamaly, R. G. Elliman, D. R. McKenzie, and S. Bulcock, Appl. Phys. A **69**, S755 (1999).

[18] A. V. Rode, E. G. Gamaly, and B. Luther-Davies, Appl. Phys. A **70**, 135 (2000).

[19] Lawrence Livermore National Laboratory, Science and Technology WWW site. http://www-cms.llnl.gov/s-t/aerogels_guinness.html.

[20] A. V. Rode, R. G. Elliman, E. G. Gamaly, A. I. Veinger, A. G. Christy, S. T. Hyde, and B. Luther-Davies, Appl. Surf. Sci. **197-198**, 644 (2002).

[21] E. G. Gamaly and A. V. Rode, *Nanostructures created by lasers*, in: *Encyclopaedia of Nanoscience and Nanotechnology*, edited by H. S. Nalwa (American Scientific Publishers, Stevenson Range, 2004), Vol. 7, pp. 783–809.

[22] B. Luther-Davies, V. Z. Kolev, M. J. Lederer, N. R. Madsen, A. V. Rode, J. Giesekus, K.-M. Du, and M. Duering, Appl. Phys. A **79**, 1051 (2004).

[23] D. Vanderbilt and J. Tersoff, Phys. Rev. Lett. **68**, 511 (1991).

[24] D. D. Berger, D. R. McKenzie, and P. J. Martin, Philos. Mag. Lett. **57**, 285 (1988).

[25] R. F. Egerton, *Electron Energy-Loss Spectroscopy in the Electron Microscope*, 2nd ed. (Plenum Press, New York, 1996).

[26] D. Arčon, Z. Jagličič, A. Zorko, and T. Makarova (unpublished).

[27] H. Katoh, Y. Hosokoshi, K. Inoue, and T. Goto, J. Phys. Soc. Jpn. **69**, 1008 (2000).

[28] A. W. Mombrú, H. Pardo, R. Faccio, O. F. de Lima, E. R. Leite, G. Zanelatto, A. J. C. Lanfredi, C. A. Cardoso, and F. M. Araújo-Moreira, Phys. Rev. B **71**, 100404(R) (2005).

[29] B. Martinez, X. Obradors, ll. Balcells, A. Rouanet, and C. Monty, Phys. Rev. Lett. **80**, 181 (1998).

[30] K. H. Fischer and J. A. Hertz, *Spin Glasses* (Cambridge University Press, Cambridge, 1991).

[31] Y. Shibayama, H. Sato, T. Enoki, and M. Endo, Phys. Rev. Lett. **84**, 1744 (2000).

[32] R. Höhne, K.-H. Han, P. esquinazi, A. Setzer, H. Semmelhack, D. Spemann, and T. Butz, J. Magn. Magn. Mater. **272-276**, e839 (2004).

[33] U. Narkiewicz, N. Guskos, W. Arabczyk, J. Typek, T. Bodziony, W. Konicki, G. Gasiorek, I. Kucharewicz, and E. A. Anagnostakis, Carbon **42**, 1127 (2004).

[34] N. Guskos, E. A. Anagnostakis, V. Likodimos, T. Bodziony, J. Typek, M. Maryniak, U. Narkiewicz, I. Kucharewicz, and S. Waplak, J. Appl. Phys. **97**, 0243404 (2005).

[35] T. Bodziony, N. Guskos, Z. Roslaniec, U. Narkiewicz, M. Kwiatkowska, and M. Maryniak, Acta Phys. Pol. A **108**, 297 (2005).

[36] A. Sadki, Y. Bounouh, M. L. Theye, J. von Bardeleben, J. Cernegora, and J. L. Fave, Diamond Relat. Mater. **5**, 439 (1996).

[37] M. Collins, R. C. Barklie, J. V. Anguita, J. D. Carey, and S. R. P. Silva, Diamond Relat. Mater. **9**, 781 (2000).

[38] J. Ristein, J. Schöfer, and L. Ley, Diamond Relat. Mater. **4**, 508 (1995).

[39] T. L. Makarova, B. Sundqvist, R. Höhne, P. Esquinazi, Y. Kopelevich, P. Scharff, V. Davydov, L. S. Kashevarova, and A. V. Rakhmanina, Nature (London) **440**, 707 (2006).